

Electrically tunable extraordinary optical transmission gratings

E. A. Shaner^{a)} and J. G. Cederberg
Sandia National Laboratories, P.O. Box 5800, Albuquerque, New Mexico 87185, USA

D. Wasserman
Department of Electrical Engineering, Princeton University, Princeton, New Jersey 08544, USA

(Received 27 August 2007; accepted 11 October 2007; published online 31 October 2007)

We report a semiconductor based mechanism for electrically controlling the frequency of light transmitted through extraordinary optical transmission gratings. In doing so, we demonstrate active control over the surface plasmon (SP) resonance at the metal/dielectric interface. The gratings, designed to operate in the midinfrared spectral range, are fabricated upon a doped GaAs epilayer. Tuning of over 25 cm^{-1} is achieved, and the devices are modeled to investigate the physical origin of the tuning mechanism. Though our structures are designed for the midinfrared, the tuning mechanism demonstrated could be applied to other wavelength ranges, especially the visible and near infrared. © 2007 American Institute of Physics. [DOI: 10.1063/1.2804572]

Perforated metal films can exhibit extraordinary optical transmission (EOT) where, at certain wavelengths, more light passes through the sample than predicted by aperture theory.¹ The majority of the work with EOT has been performed in the visible and near-infrared (near-IR) spectral regions. However, as midinfrared (mid-IR, 3–30 μm wavelength) sources steadily and rapidly improve, the burgeoning field of mid-IR photonics is presenting numerous opportunities for EOT technology and research. While current work with passive EOT structures has shown great promise, the ability to electrically tune such devices would add greater functionality to a variety of photonic applications. In previous work, we have shown that changing the carrier concentration in GaAs epilayers can shift the transmission peak of mid-IR EOT structures.² For *n*-type doping densities varying from 1×10^{16} to $3 \times 10^{18}\text{ cm}^{-3}$, a shift of 0.14 μm (22 cm^{-1}) was achieved for gratings transmitting at 8 μm (1250 cm^{-1}). While this previous work achieved EOT peak shifts utilizing separate samples, we show in this letter that even greater shifts can be achieved from a single device using electronically controlled current tuning of the EOT structure.

The sample studied, shown in Figs. 1(a) and 1(b), was grown by metal-organic chemical vapor deposition and consists of a 100 nm thick *n*-doped ($3.5 \times 10^{18}\text{ cm}^{-3}$) GaAs epilayer above an undoped 50 nm $\text{Al}_{0.2}\text{Ga}_{0.8}\text{As}$ epilayer and an undoped GaAs buffer layer on a semi-insulating GaAs substrate. Fabrication of the device, shown in Fig. 1(a), consisted of a mesa etch through the doped epilayer, followed by evaporation and annealing of Ohmic (235 Å Ge/470 Å Au/300 Å Ni/1000 Å Au) source and drain contacts. A 10 nm/50 nm Ti/Au square lattice grating designed for transmission at 8 μm (2.4 μm period and 1.25 μm holes) was then defined using optical photolithography and a lift-off metallization process. While this is not an optimum metallization for mid-IR surface plasmons (SPs), previous work has shown that Ti/Au meshes exhibit EOT phenomena.² Light transmission through such a structure relies on SP excitations at the air/metal and the metal/dielectric interfaces. An approximate expression for the normal incidence SP resonance

condition, based on the SP dispersion of a smooth metal film, is given by^{3,4}

$$\sqrt{i^2 + j^2}\lambda = a_0 \text{Re} \left(\sqrt{\frac{\epsilon_s \epsilon_m}{\epsilon_s + \epsilon_m}} \right). \quad (1)$$

Here, λ is the free space wavelength, a_0 is the lattice constant (2.4 μm), i and j are integers related to the reciprocal lattice vectors $2\pi/a_0 \mathbf{x}$ and $2\pi/a_0 \mathbf{y}$, respectively, and ϵ_s and ϵ_m are the complex permittivities of the semiconductor (or air) and metal, respectively. The spectral position of the transmission peak related to the metal/semiconductor SP can be tuned by varying a_0 or ϵ_s . When current is passed under the metal mesh, as shown in Fig. 1(c), the epilayer is resistively heated, tuning both of these parameters, to varying degrees, simultaneously.

The normalized mid-IR transmission for our device as a function of electrical current is displayed in Fig. 2. Mid-IR transmission data was collected with a Fourier transform infrared spectrometer using an external, liquid-nitrogen cooled mercury cadmium telluride detector. Spectral resolution of 2 cm^{-1} was used and the data was averaged over 25 scans.

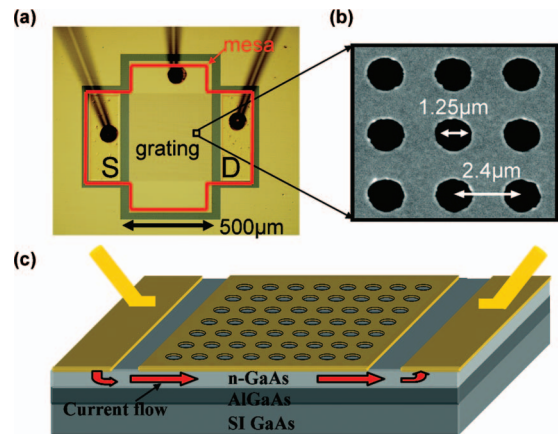


FIG. 1. (Color) Tunable midinfrared extraordinary transmission device. (a) Optical micrograph of tunable EOT device with labeled source contact (S), drain contact (D), and grating. (b) Scanning electron micrograph of transmission grating designed for transmission at 8 μm . (c) Schematic of tunable EOT device showing current path through *n*-doped GaAs epilayer, source and drain contacts, and transmission grating (not to scale).

^{a)}Electronic mail: eashane@sandia.gov

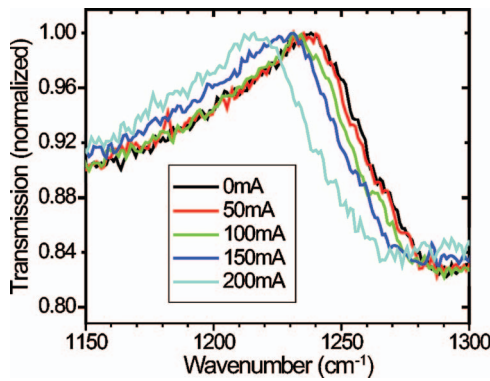


FIG. 2. (Color) Transmission spectra showing peak shift with current. Normalized transmission spectra for $8 \mu\text{m}$ tunable surface plasmon device as a function of source-drain current. A clear redshift can be seen as the current is increased from 0 to 200 mA. The maximum shift achieved was 25 cm^{-1} .

Current was applied between the source and drain contacts using a dc power supply operating in constant current mode. Data collection was initiated upon stabilization of the source-drain voltage (approximately 1–5 s). The transmission spectra exhibit the Fano-lineshape associated with EOT structures.⁵ The relatively large background signal ($\sim 84\%$) is due to the light transmission through the nonmetalized areas that can be seen in Fig. 1(a) along the perimeter of the Ohmic contacts and the mesh. A transmission peak redshift of approximately 25 cm^{-1} is achieved as the source-drain current is tuned from 0 to 200 mA (0 to 1.86 W power dissipated). The strength of the transmission peak does not decrease substantially ($\sim 25\%$ reduction) at the highest current. Additionally, we see no increase in the peak linewidth as a function of current. Both of these results suggest that scattering and free carrier losses do not significantly affect device performance at high temperatures. The tuning achievable with such a configuration, in addition to the stable transmission strength and linewidth, suggests that such devices could be utilized as actively tunable mid-IR optical components.

A number of mechanisms are associated with temperature changes that can cause the observed shift. To accurately model these, the temperature of the device as a function of current must be determined. Temperature calibration was obtained by band edge photoluminescence (PL) spectroscopy. As the current is increased and the sample is heated, the semiconductor band edge shifts, as shown in the inset of Fig. 3. By tracing the position of the GaAs band edge PL as a function of current, an approximate value for the device temperature is found using the empirical relation for the temperature (Kelvin) dependence of the GaAs band gap (eV),⁶

$$E_G(T) = 1.519 - 5.405 \times 10^{-4} T^2 / (T + 204). \quad (2)$$

As shown in Fig. 3, the temperature of the device can be tuned from 300 K (0 mA) to over 550 K (200 mA).

From a geometrical standpoint, thermal expansion can change a_0 which, according to Eq. (1), would lead to a redshift in the SP transmission peak. However, this is only a small effect ($\sim 2 \text{ cm}^{-1}$) at the highest temperatures. In our semiconductor medium, there are several competing temperature dependent dielectric shifts. In the undoped material, we must consider the thermal generation of free carriers and the temperature dependence of the dielectric constant. In the relatively thin doped layer, which contains a high density of built-in free carriers, these effects must be considered along

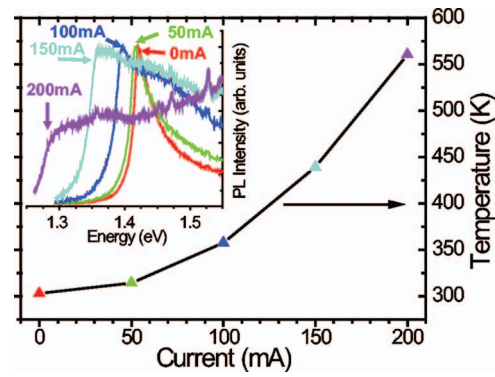


FIG. 3. (Color) Device surface temperature derived from photoluminescence spectra (inset) as a function of current. For a fixed current, photoluminescence was used to relate the position of the GaAs band edge to the device temperature. The main plot shows the resulting temperature calibration obtained using this method.

with the reduction of both the semiconductor plasmon damping time and the free carrier effective mass. The thin $\text{Al}_{0.2}\text{Ga}_{0.8}\text{As}$ layer, having optical properties very similar to GaAs (Ref. 7) (and because it is very thin compared to the wavelengths of interest), is modeled together with the undoped GaAs buffer layer for simplification.

The temperature dependence of the semiconductor dielectric function can be modeled using the Drude approximation, including scattering, as

$$\varepsilon(\omega, T, n) = \varepsilon_b(T) \left[1 - \frac{\omega_p(T, n)^2}{\omega^2 + i\omega\gamma(T, n)} \right],$$

$$\omega_p(T, n)^2 = \frac{4\pi n(T)e^2}{\varepsilon_b(T)m^*(T, n)}. \quad (3)$$

Here, $\omega_p(T, n)$ is the plasma frequency, $\gamma(T, n)$ is the plasmon damping term ($=1/\tau$, where τ is the scattering time), $n(T)$ is the carrier concentration, e is the charge of an electron, $\varepsilon_b(T)$ is the background high frequency dielectric constant of the semiconductor, and $m^*(T, n)$ is the effective electron mass in the semiconductor. In Fig. 4(a), the shift of the SP resonance is modeled using Eq. (1) with a Au mesh and the temperature and doping dependent relationships for the above parameters (m^* , ω_p , γ , n , and ε_b).^{6,8} The modeled shift is greatest for the undoped GaAs buffer and substrate, and is explained by the temperature dependence of the GaAs dielectric constant,⁶

$$\varepsilon_b(T) = 10.6(1 + T \cdot 9 \times 10^{-5}). \quad (4)$$

Thermal generation of carriers can only create bulk densities on the order of $1 \times 10^{13} \text{ cm}^{-3}$ at our elevated temperatures, which is orders of magnitude too low to provide any noticeable shifting of the SP peak. The additional temperature dependent terms in Eq. (3) do, however, affect the peak position expected at higher temperatures for doped material. In Fig. 4(a), as the doping of the semiconductor is increased, the redshift of the transmission peak is somewhat offset by the Drude contribution to the dielectric function.

Figure 4(b) shows the calculated redshift for an $8 \mu\text{m}$ grating device (black dashed) assuming an undoped GaAs dielectric along with the measured peak positions (red). Since the redshift in our devices is greater than that predicted by temperature tuning of the undoped dielectric, it is argued that the majority of the metal/semiconductor SP field lies in

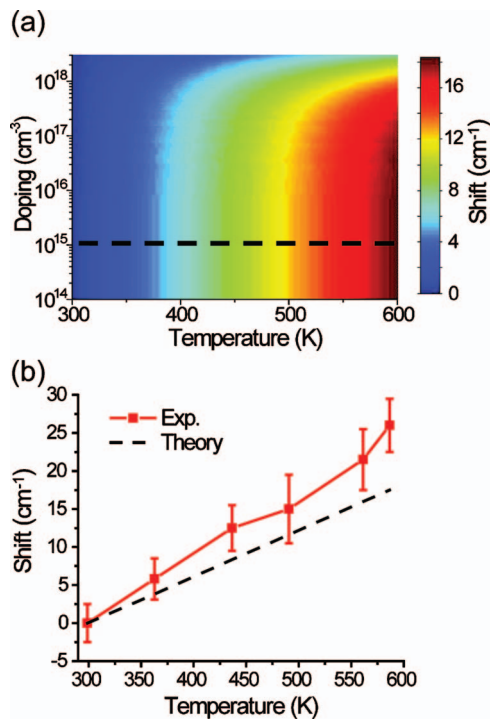


FIG. 4. (Color) Calculated and experimental redshift of tunable SP grating devices as a function of temperature. (a) The calculated magnitude of the spectral shift as a function of both doping and temperature. As the doping is increased, less of a redshift is expected. (b) The calculated (black dashed) and experimental (red solid) redshifts. The calculated curve in (b) also corresponds to the black dashed line in (a) where the doping is low enough to have a negligible effect.

the undoped material, and the thin, highly doped GaAs layer serves mostly as a heating mechanism with minimal influence over the SP transmission peak spectral position.

To utilize these tunable plasmonic devices as active optical components, the effect of losses on the transmission intensity and the linewidth of the transmission peak must be addressed. As mentioned earlier, a decrease in transmission peak strength of $\sim 25\%$ is seen as the device temperature is increased. This is most likely due to increased losses in both the $500\ \mu\text{m}$ GaAs substrate and at the interface between the metal mesh and the highly doped GaAs epilayer. Burying the doped GaAs layer under an undoped surface layer would decrease the overlap of the SP field with the free carriers of the doped layer, while still allowing for resistive heating of the sample. Substrate losses can be minimized by moving toward thinner devices which, at the same time, will reduce

the thermal mass and electrical power requirements. Finally, the linewidth and shape of the transmission peak can also be significantly improved by utilizing the crossed-polarizer experimental configuration employed by Pang *et al.*⁵ We have performed such an experiment on large area SP gratings and have seen linewidths of less than $10\ \text{cm}^{-1}$ for EOT gratings designed for transmission at $9\ \mu\text{m}$ ($1111\ \text{cm}^{-1}$).

In conclusion, we have demonstrated electrically controlled temperature tuning of transmission through extraordinary optical transmission gratings in the midinfrared. We have shown tuning of over $25\ \text{cm}^{-1}$ by adjusting the current beneath the metal/dielectric interface. The dielectric properties of both the doped heater layer and the undoped substrate were analyzed in order to understand the origins of the transmission tuning. The development of semiconductor based tuning mechanisms for mid-IR SP resonances is important for a variety of active mid-IR photonic devices including filters, emitters, and detectors. However, it should be noted that this work has implications for a broad range of frequencies, as the mechanisms investigated could be utilized in the near-IR and visible (with a wide band gap semiconductor) wavelength ranges. The ability to design and fabricate active, electrically controlled, surface plasmon devices in the mid-IR and possibly the near-IR/visible range opens up new capabilities for plasmon-based technologies.

D.W. would like to thank the Princeton Council on Science and Technology for additional funding. The authors also thank Doug Nelson and C. Gmachl for discussion and equipment use. Sandia is a multiprogram laboratory operated by Sandia Corporation, a Lockheed Martin Company, for the United States Department of Energy's National Nuclear Security Administration under Contract No. DE-AC04-94AL85000.

¹T. W. Ebbesen, H. J. Lezec, H. F. Ghaemi, T. Thio, and P. A. Wolff, *Nature* (London) **391**, 667 (1998).

²D. Wasserman, E. A. Shaner, and J. G. Cederberg, *Appl. Phys. Lett.* **90**, 191102 (2007).

³H. F. Ghaemi, T. Thio, D. E. Grupp, T. W. Ebbesen, and H. J. Lezec, *Phys. Rev. B* **58**, 6779 (1998).

⁴K. R. Rodriguez, H. Tian, J. M. Heer, and J. V. Coe, *J. Phys. Chem.* **111**, 12106 (2007).

⁵L. Pang, K. A. Tetz, and Y. Fainman, *Appl. Phys. Lett.* **90**, 111103 (2007).

⁶J. S. Blakemore, *J. Appl. Phys.* **53**, R123 (1982).

⁷S. Gehrsitz, F. K. Reinhart, C. Gourgon, N. Herres, A. Vonlanthen, and H. Sigg, *J. Appl. Phys.* **87**, 7825 (2000).

⁸K. H. Nichols, C. M. L. Yee, and C. M. Wolfe, *Solid-State Electron.* **23**, 109 (1980).